Supporting Information

In situ Control of pH using a Boron Doped Diamond Ring Disk Electrode: Optimizing Heavy Metal (Mercury) Detection

Tania L. Read, Eleni Bitziou, Maxim B. Joseph, and Julie V. Macpherson*

Department of Chemistry, University of Warwick, Coventry, CV4 7AL

Table of Contents

S1. FEM simulation of H^+ generation at the ring disk electrode

S2. Electrochemical characterization of the BDD ring disk electrode

S3. FEM simulations of the *r,z* pH profile for i_{ring} = +50 μA (ring) and t = 1, 5, 10, 30 and 600 s.

S4. FEM simulations of the *r,z* pH profiles for t = 60 s and i_{ring} = +10, +20, +30 and +40 μA.

S1. FEM simulation of H^+ generation at the ring disk electrode

To quantify pH changes across the detector electrode in response to the diffusional flux of H^+ generated at the ring electrode, a finite element model (FEM) was employed using COMSOL Multiphysics 4.3a (COMSOL AB, Sweden) software. A schematic of the simulated domain is shown in Figure S1. The model consisted of a square box of width (w_T) = 50 mm and height (h) = 50 mm, with coordinates r and z respectively, producing a 2D axisymmetric section defined by four boundaries, 1, 2, 3 and 4, and representing a water cylinder. The ring disk system is defined by subdividing boundary 1; the disk (boundary 1a) is defined by w_1 (r = 0.461 mm) and the ring (boundary 1c) is defined by the distance between w_2 and w_3 (r = 0.723 mm and r = 0.873 mm, respectively), the remainder of boundary 1 represents the insulating epoxy surface (boundary 1b). These dimensions are representative of the experimental system.

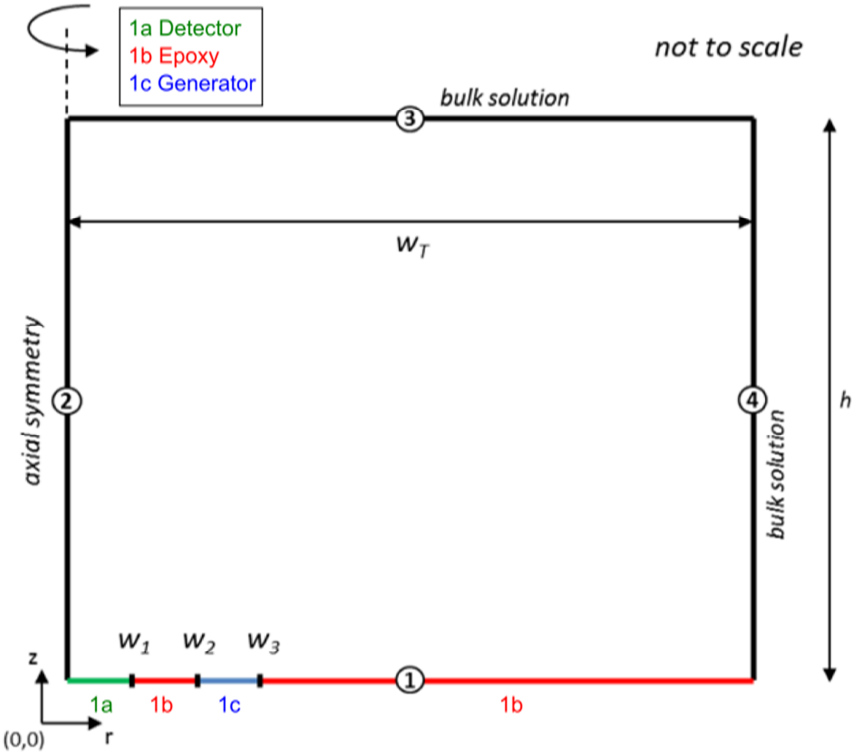

Figure S1: Schematic diagram of the simulation domain; an axisymmetric section of a water cylinder on top of a ring disk electrode arrangement defined by points $w_{1\text{-}3}$ and lengths h and w_T.

The size of the box is chosen such that the diffusion of generated H^+ does not reach the edge on the timescale of the simulation. 1a, the disk electrode, is assumed to be electrochemically inert (*i.e.* no electrolysis of H^+; no flux, *vide infra*), as is 1b, which is made from insulating material. 1c, the ring electrode, has an inward flux defined across the surface corresponding to the generation of H^+ by electrolysis of water.

The flux is assumed to be proportional to the galvanostatic current flowing at the ring electrode;

$$\mathbf{n}\cdot\mathbf{N}_{1c} = \frac{i_{ring}}{A\cdot F} \qquad \text{(S1)}$$

where **n** is the unit normal vector, $\mathbf{N}_p$ is the total inward flux across boundary 1c, i_{ring} is the total current at the electrode, A is the area of the electrode and F is Faraday's constant (=96485 C mol^{-1}). Boundaries 3 and 4 were defined as having a fixed $[H^+]$ of $10^{-6.4}$ M (bulk pH 6.4), while boundary 2 was defined by an axisymmetric constraint. The diffusion coefficient of H^+ (D_p) was set to 9.31 x 10^{-5} cm^2 s^{-1} in accordance with the literature[1] and the initial concentration of H^+ c_p was set to $10^{-6.4}$ M, corresponding to the bulk pH of the experimental solution (see main text).

Diffusion of H^+ from the generator electrode was modeled according to Fick's second law;

$$\frac{\partial c_p}{\partial t} = D_p \nabla^2 c_p \qquad \text{(S2)}$$

A mesh was generated with an element length of 2 μm at sub-boundaries 1a, 1b and 1c; the remaining domain was meshed continuously at a growth rate of 1.01 × per element away from these boundaries to a maximum element size of 0.5 mm. The total mesh consisted of 461,389 elements. The simulation was solved in a time-dependent manner for a total of 600 s using the PARDISO solver as implemented in COMSOL.

Table S1. Summary of boundary conditions used for the simulation of the pH during the ring generation experiment

Boundary	Boundary type	Coordinates	Equation
1a	Disk Electrode	$0 \le r \le w_1$ $z = 0$	$0 = \nabla c \cdot \mathbf{n}$
1b	Epoxy mount material	$w_1 \le r \le w_2$ *and* $w_3 \le r \le w_T$ $z = 0$	$0 = \nabla c \cdot \mathbf{n}$
1c	Generator ring	$w_2 \le r \le w_3$ $z = 0$	$\mathbf{n} \cdot \mathbf{N}_{1c} = \frac{i}{A \cdot F}$
2	Axis of symmetry	$r = 0$ $0 \le z \le h$	$0 = \nabla c \cdot \mathbf{n}$
3	Bulk solution	$0 \le r \le w_T$ $z = h$	$c = c^*$
4	Bulk solution	$r = w_T$ $0 \le z \le h$	$c = c^*$

In table S1, $\mathbf{N}_{1c}$ represents the total inward flux across the boundary 1c, and c^* represents the concentration of the electroactive species in the bulk solution.

S2. Electrochemical characterisation of the BDD ring disk electrode

The individually addressable BDD ring disk electrode was electrochemically characterized using the fast one electron transfer outer sphere redox couple (1 mM) $Ru(NH_3)_6^{3+}$ in 0.1 M KNO_3. Figure S2 shows typical CVs for the disk and ring electrode (left and right respectively) over the potential scan rate range, *v,* 10 mV s^{-1} to 500 mV s^{-1}. For the electrode sizes employed, near reversible peak-to-peak voltage separations (ΔEp) were obtained indicating close to reversible behavior, as expected.[2] For example, at 50 mV s^{-1} and 100 mV s^{-1} the ring and the disk electrodes showed values of 75 mV (50 mV s^{-1}) and 69 mV (100 mV s^{-1}), and 69 mV (50 mV s^{-1}) and 70 mV (100 mV s^{-1}) respectively.

Plots of peak current, i_p versus $v^{1/2}$ gave straight lines with gradients 7.65×10^{-6} A $(V\ s^{-1})^{-1/2}$ and 9.15×10^{-6} A $(V\ s^{-1})^{-1/2}$ and R^2 values 0.9997 and 0.9993 for ring and disk electrodes respectively. For the electrode geometries used planar diffusion was expected to dominate on the experimental timescales explored,[3] in accordance with the linear relationship between i_p and $v^{1/2}$. Randles Sevcik analysis gave an effective electrode radius for the disk = 0.56 mm (assuming D = 8.8 x 10^{-6} $cm^2\ s^{-1}$)[4] slightly larger than expected. This suggests that the BDD disk is protruding slightly from the insulating epoxy surround,[3] which is not surprising as during fabrication the epoxy polishes at a much faster rate than the BDD.

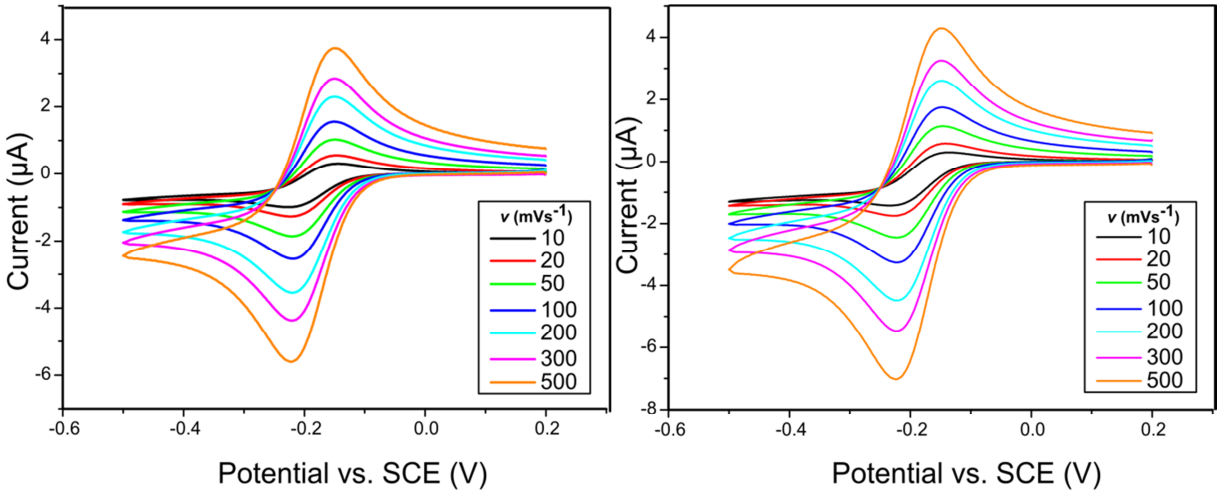

Figure S2: CVs in 1 mM $Ru(NH_3)_6^{3+}$ for the BDD disk (left) and ring (right) electrodes at scan rates in the range 10 – 500 mV s^{-1}.

S3. FEM simulations of the *r,z* pH profile for i_{ring} = +50 μA (ring) and *t* = 1, 5, 10, 30 and 600 s.

The diffusion of H^+ from the ring across the surface of the disk and into the bulk solution was simulated as described in S1. *r,z* plots of the pH profile for the ring disk dimensions given in S1 for i_{ring} = +50 μA and t = 1, 5, 10, 30, 60 and 600 s are shown in Figures S4a-f respectively. The pH profile over the disk electrode changes rapidly during the first 30 s (as shown in Figures S3a – d) as H^+ transit from the ring to the disk. For t > 30 s the change in

pH profile in the vicinity of the disk is far less dramatic and reaches a steady-state pH value of 2.0, as shown here and in the pH-time profiles displayed in Figure 2c in the main text.

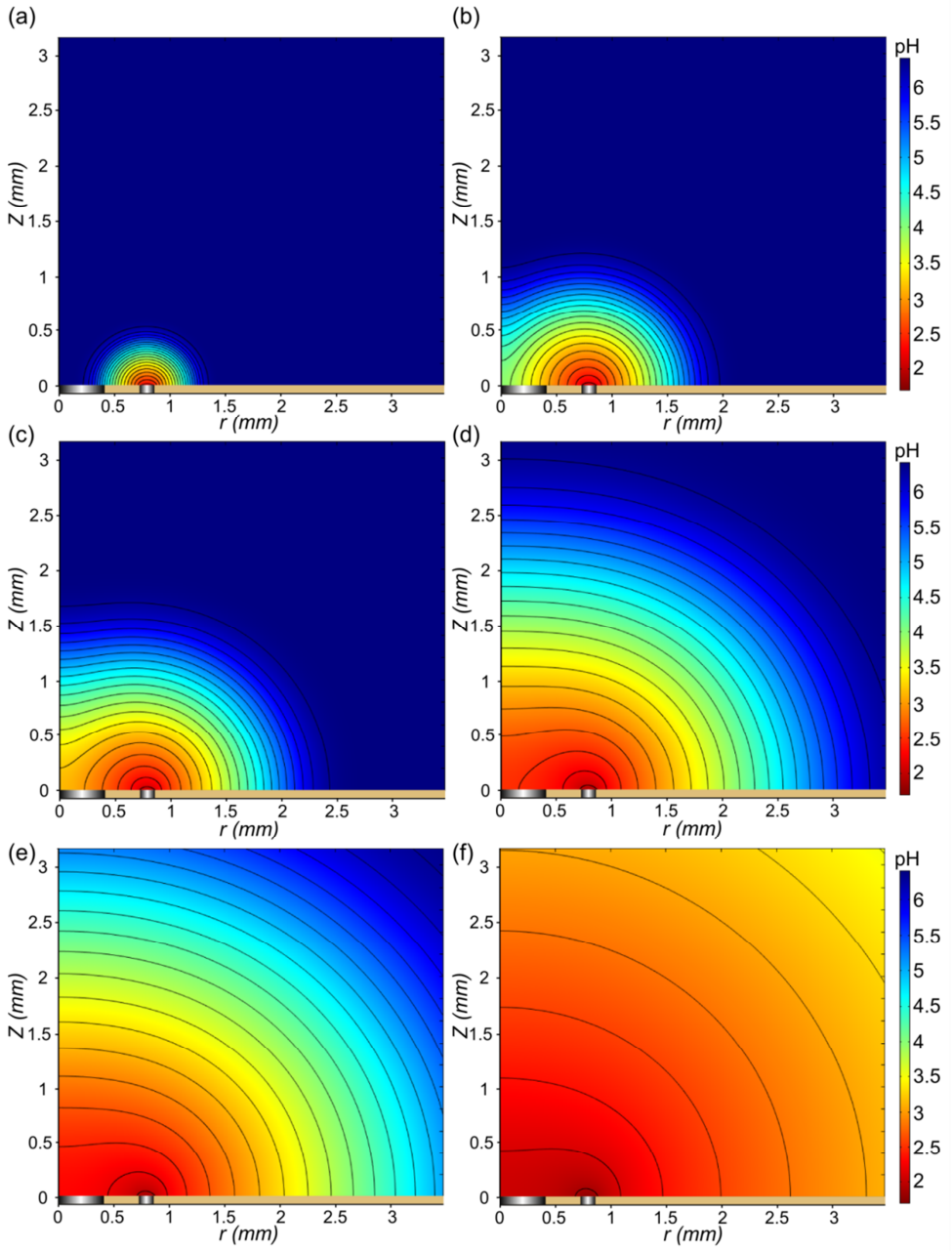

Figure S3: Simulated pH profiles for i_{ring} =+50 μA at t = (a) 1 s, (b) 5 s, (c) 10 s, (d) 30 s, (e) 60 s, and (f) 600 s, showing the evolution of the pH profile with time. The pH color scale is identical for all six profiles and the ring and disk placements are illustrated above the r axis.

S5. FEM simulations of the r,z pH profiles for time = 60 s and ring currents, +10, +20, +30 and +40 μA.

Figure S5 shows the change in *r,z* pH profile for t = 60 s as i_{ring} is increased from (a) +10 μA; (b) +20 μA: (c) +30 μA to (d) +40 μA. As the galvanostatic current is increased, the flux of H^+ from the ring increases, resulting in a lower pH recorded at the disk electrode (Figure 2c).

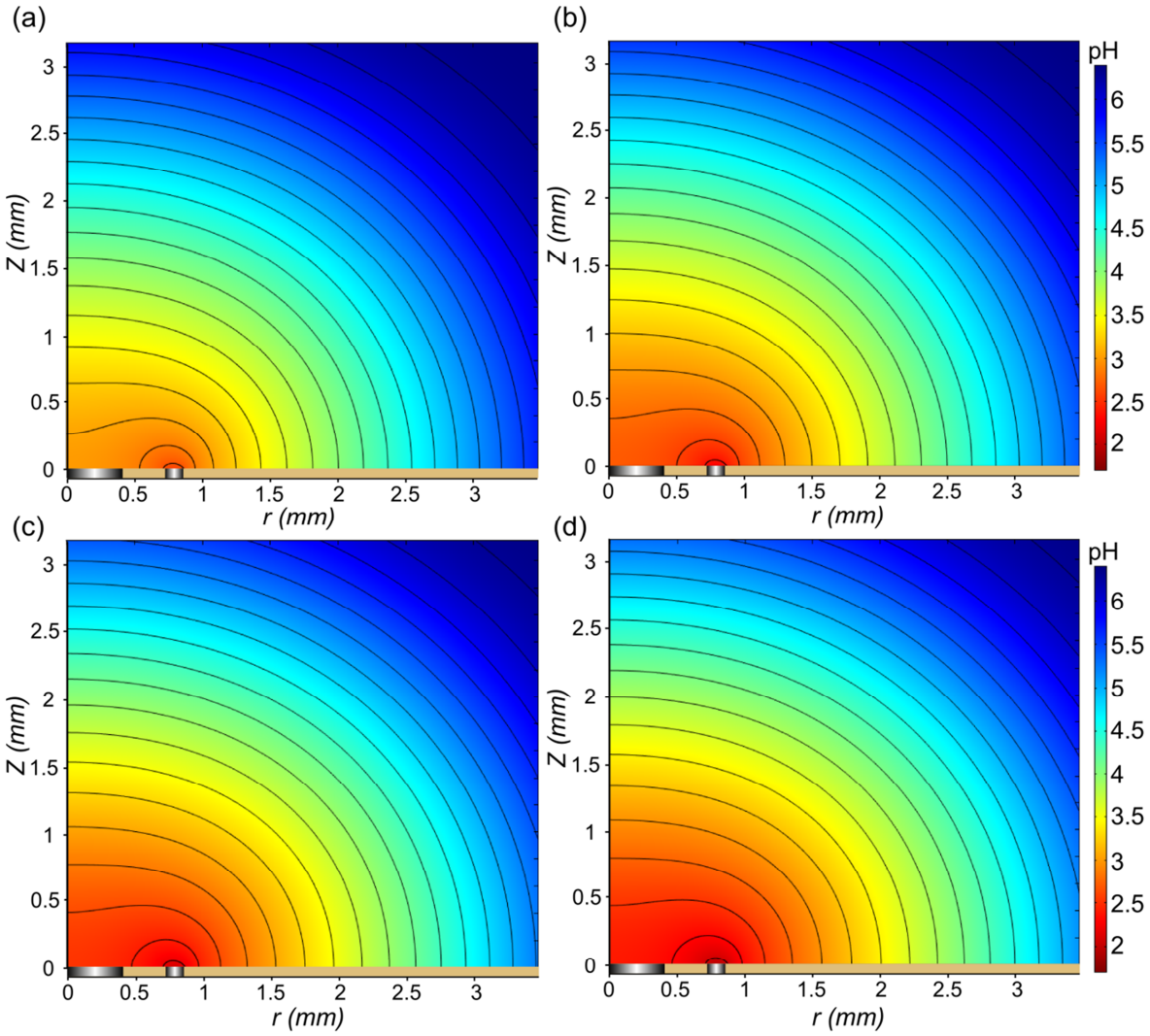

Figure S5: Simulated pH profiles after 60 s generation for i_{ring} = (a)+ 10 μA, (b)+ 20 μA, (c)+ 30 μA, and (d)+ 40 μA. The pH color scale is identical for all four profiles and the ring and disk placements are illustrated above the r axis.

References

(1) Robinson, R. A.; Stokes, R. H. *Electrolyte Solutions*; Butterworth. 1959.
(2) Patten, H. V.; Meadows, K. E.; Hutton, L. A.; Iacobini, J. G.; Battistel, D.; McKelvey, K.; Colburn, A. W.; Newton, M. E.; Macpherson, J. V.; Unwin, P. R. *Angewandte Chemie*, **2012**, *124*, 7108-7112.
(3) Ferrigno, R.; Brevet, P.; Girault, H. *Electrochim. Acta*, **1997**, *42*, 1895-1903.
(4) Macpherson, J. V.; O'Hare, D.; Unwin, P. R.; Winlove, C. P. *Biophysical Journal*, **1997**, *73*, 2771-2781.